International Journal of Pure and Applied Mathematics
Volume 53 No. 3 2009, 333-353

A LEVEL SET REACTION-DIFFUSION MODEL FOR TISSUE REGENERATION IN A CARTILAGE-HYDROGEL AGGREGATE

Sarah D. Olson[1], Mansoor A. Haider[2] §

[1]Department of Mathematics
Tulane University
6823, St. Charles Ave., New Orleans, LA 70118, USA
e-mail: solson2@tulane.edu

[2]Department of Mathematics
North Carolina State University
P.O. Box 8205, Raleigh, NC 27695-8205, USA
e-mail: m_haider@ncsu.edu

Abstract: A mathematical model and numerical solutions are presented for an interface problem that models an in-vitro experiment for regeneration of articular cartilage in a localized defect region. In this experiment, a cylindrical cartilage explant has a core region removed and replaced with a nutrient-rich hydrogel. The gel-tissue aggregate is then immersed in media for a period of several weeks. An axisymmetric reaction-diffusion model of this experiment is developed to capture coupling between cell-mediated nutrient absorption and matrix biosynthesis, and diffusive transport of nutrients and matrix constituents. The reaction governing turnover of the hydrogel to newly synthesized tissue is modeled via a level set method that captures the moving gel-tissue interface, and local curvature effects are also considered. After nondimensionalization, finite difference numerical solutions are employed to simulate cartilage regeneration as a function of cell mediated reaction rates in the model. Both the cases of external media maintained at a homeostatic nutrient concentration, and at a higher concentration associated with the nutrient-rich hydrogel are considered. Via a detailed parametric analysis using the model, regeneration times required to completely degrade the hydrogel are determined. Potential effects of local curvature along the gel-tissue interface are briefly discussed.

Received: April 28, 2009

§Correspondence author

AMS Subject Classification: 92, 35, 65
Key Words: reaction-diffusion model, cartilage regeneration, level set method, tissue engineering, hydrogel, interface problem

1. Introduction

Articular cartilage is a connective tissue that lines bone surfaces in diarthrodial joints such as the knee, shoulder, and hip. Cartilage serves to protect these surfaces from impact stresses, and minimize friction and wear in the joint [4, 17]. The structure of this tissue arises from an extracellular matrix (ECM), consisting largely of water (∼80% by volume), as well as collagen, proteoglycan, and other proteins [16]. Dispersed throughout the ECM is a sparsely distributed population of cells (∼1-10% by volume), called chondrocytes [1]. Since cartilage is avascular and aneural, biophysical factors in the local cellular environment are known to play an important role in regulating cell biosynthetic activity [32]. Osteoarthritis results in structural degradation of cartilage ECM, and can give rise to holes or defects that are precursors to complete degradation necessitating joint replacement [25, 35]. Cartilage has a limited capacity for growth and repair of large defects; therefore, approaches using cellular supplementation or biomaterials for defect-filling have been developed to promote tissue maintenance or regeneration [23, 31]. Specific material types can address additional factors including promotion of cell proliferation, nutrient diffusion, and matrix biosynthesis in regions of interaction between the native tissue and the biomaterial [12, 14].

Hydrogels, which are superabsorbent, nutrient-rich natural or synthetic polymers are being explored to provide a three-dimensional scaffold for cartilage regeneration [3, 7, 18, 19]. Upon insertion into a defect, hydrogels will slowly degrade as cellular biosynthesis and proliferation result in turnover of the gel scaffold to cartilage ECM [9, 22, 24]. Since little is known about the optimal conditions for cartilage regeneration, mathematical models capturing interactions between matrix accumulation, hydrogel degradation and nutrient diffusion have potential utility in accelerating the realization of optimal strategies for cartilage repair [26]. In this study, one such model is developed for an in-vitro cartilage regeneration experiment that can be performed on a cylindrical tissue explant. In this experiment, a core region is removed from the explant and replaced with hydrogel (Figure 1). The cartilage-hydrogel aggregate is maintained in a fluid bath with adequate nutrient supply. Over the course of several weeks, cell-synthesized ECM constituents react and replace

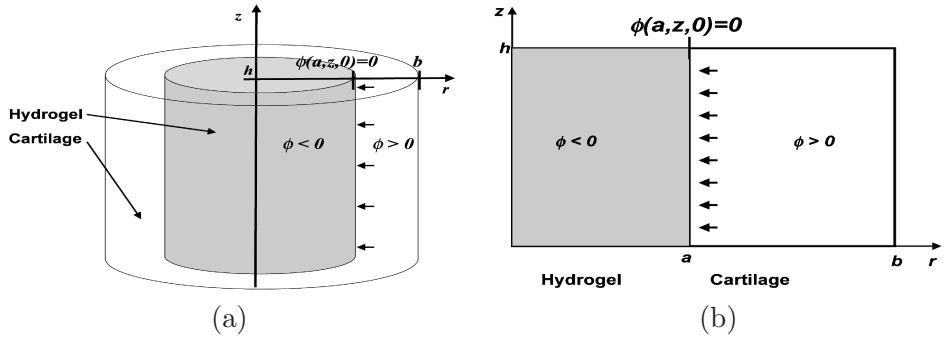

Figure 1: Depiction of the in-vitro cartilage regeneration experiment. (a) A cylindrical core is cut out of the tissue explant, replaced with a hydrogel, and the aggregate is immersed in media (b) Axisymmetric geometry is assumed, and a level set function ϕ is used to track the evolving interface between the tissue ($\phi > 0$) and hydrogel ($\phi < 0$) regions.

the hydrogel in the core region.

In this general context of cartilage tissue engineering, it is noted that previous models have considered models of matrix synthesis [10, 33], reaction-diffusion models [5, 6, 20, 27, 28], moving boundary approaches [11, 34], and models of multiphase porous mixtures [15]. Each of these models captures different aspects of cartilage regeneration through modeling matrix biosynthesis, cellular proliferation, and/or nutrient diffusion and utilization. Models by Obradovic et al [20] and Wilson et al [33] have an equation for degradation of the hydrogel scaffold but do not capture spatial effects of the interface between newly regenerated cartilage and the scaffold. A moving boundary approach by Galban et al [11] captures the location of cells growing, but does not model the nutrient or matrix concentrations.

Under the assumption of axisymmetric geometry we present a reaction-diffusion model for in-vitro tissue regeneration in a two-zone, hydrogel-tissue aggregate. Associated numerical solutions are also developed in which the location of the reacting interface between the hydrogel and cartilage regions is captured using a level set method. A primary modeling goal is to analyze effects of model parameters on the tissue regeneration time, i.e. the time required to replace the hydrogel with cell-synthesized ECM.

2. Cartilage Regeneration Model

2.1. Motivation and Assumptions

We model an in-vitro experiment in which a cylindrical cartilage explant has a core cylindrical region cut-out, and the hole is filled with a hydrogel sample that matches the shape of the defect (Figure 1). The gel-tissue aggregate is then immersed in media with the lower face of the aggregate ($z = 0$) supported by an impermeable platen. Over the course of multiple weeks, nutrient diffusion into the cartilage region stimulates cell proliferation and cellular biosynthesis of ECM constituents. As the newly synthesized ECM constituents diffuse into their surroundings, in the hydrogel region, they react with the gel polymer to replace it with newly formed tissue, i.e. ECM and cells. Of primary interest to the experimentalist is the time required to regenerate the tissue via complete turnover of the hydrogel volume to new cartilage as the phenomenon proceeds.

To simplify this complex biophysical problem, we idealize the gel-tissue aggregate as a reaction-diffusion system with a nutrient concentration variable N and a matrix accumulation variable M that vary spatially and evolve in time. Nutrient concentrations above a homeostatic level are assumed to result in cell absorption of nutrients that induce net matrix synthesis relative to a homeostatic matrix density. The reaction that results in replacement of hydrogel with newly synthesized cartilage is idealized via a level set model of the gel-tissue interface with propagation speed proportional to quantities that drive the reaction. We assume that, as the interface advances into the hydrogel region, the additional volume of synthesized cartilage left behind preserves the cell density in the original explant via cell proliferation. Nutrients and accumulated matrix are free to diffuse in both the hydrogel and cartilage regions, but we idealize the gel-tissue reaction as localized to the interface, motivated by the capability of nearby cells to drive this reaction. Thus, our model considers coupling between mechanisms of diffusive nutrient and accumulated matrix transport, nutrient absorption and net matrix synthesis by the cells (cartilage region), and reaction phemomena at the gel-tissue interface. A primary goal is to understand effects of these coupled mechanisms on the *regeneration time* that is required to replace the entire hydrogel region with newly synthesized cartilage.

2.2. Level Set Reaction-Diffusion Model

Introducing cylindrical coordinates (r, θ, z), we assume that all quantities are independent of θ. In our model, the primary variables of interest are the time-varying *nutrient concentration* $N(r, z, t)$, the *net matrix accumulation* $M(r, z, t)$, which is taken to be zero in a state of cartilage homeostasis, and the *level set function* $\phi(r, z, t)$ [21] which governs the location of the evolving gel-tissue interface via the level set $\phi(r, z, t) = 0$. Note that the cartilage and hydrogel regions correspond to $\phi > 0$ and $\phi < 0$, respectively (Figure 1).

The following reaction-diffusion equation is proposed to model diffusive nutrient transport and cellular consumption of nutrients ($0 < r < b, 0 < z < h, t > 0$):

$$\frac{\partial N}{\partial t} = D_N^{(i)} \left(\frac{\partial^2 N}{\partial r^2} + \frac{1}{r}\frac{\partial N}{\partial r} + \frac{\partial^2 N}{\partial z^2} \right) - k_N^{(i)}(N - N^*)\,, \tag{1}$$

where:

$$i = \begin{cases} 1 & \phi(r, z, t) < 0 \text{ (hydrogel)}\,, \\ 2 & \phi(r, z, t) > 0 \text{ (cartilage)}\,, \end{cases} \qquad k_N^{(1)} = 0\,. \tag{2}$$

The choice $k_N^{(1)} = 0$ is made, corresponding to the assumption that the hydrogel region does not contain cells during the entire course of the regeneration experiment. Within the cartilage region, the cell utilization rate of nutrients, $k_N^{(2)}$, is assumed to be proportional to the excess relative to a homeostatic concentration, N^*. This relative measure will also couple to a second equation for net matrix accumulation via upregulated synthesis of ECM constituents by the cartilage cells as nutrients are absorbed.

Consequently, a second reaction-diffusion equation, that is coupled to (1), is introduced to model synthesis of ECM by the cells in the cartilage region and diffusive transport through both regions ($0 < r < b, 0 < z < h, t > 0$):

$$\frac{\partial M}{\partial t} = D_M^{(i)} \left(\frac{\partial^2 M}{\partial r^2} + \frac{1}{r}\frac{\partial M}{\partial r} + \frac{\partial^2 M}{\partial z^2} \right) + k_M^{(i)}(N - N^*), \quad k_M^{(1)} = 0\,. \tag{3}$$

In (3), it is noted that matrix synthesis is initiated when the nutrient concentration is in excess of its homeostatic value N^*. Due to the assumption of no cells in the hydrogel region, the choice $k_M^{(1)} = 0$ is also made. For the case of a cartilage sample with no hydrogel that is immersed in a bath at nutrient concentration N^*, note that the model (1)-(3) reduces to the homeostatic equilibrium state with nutrient concentration $N(r, z, t) = N^*$ and no net ECM synthesis, i.e. $M(r, z, t) = 0$.

The final equation in our model governs the interaction at the gel-tissue interface that causes accumulated ECM to replace degraded hydrogel via a local reaction that is mediated by nearby cells. We idealize this interaction as a local interfacial phenomenon on the level set $\phi(r,z,t)=0$ that is embedded in a higher dimensional level set function $\phi(r,z,t)$ [21]. We assume that the reaction proceeds according to the relation $(0<r<b, 0<z<h, t>0\ )$:

$$\frac{\partial \phi}{\partial t}+\mathbf{V}\cdot\nabla\phi=\frac{\partial \phi}{\partial t}+F|\nabla\phi|=0\,,\qquad \text{where:}\quad \mathbf{V}=F\mathbf{n}=F\frac{\nabla\phi}{|\nabla\phi|}\,. \tag{4}$$

In (4), the gel-tissue turnover is assumed to occur in a direction $\mathbf{n}$ that is locally normal to the interface, and at a reaction rate F that depends on several local variables in the model. We assume that the gel-tissue reaction rate is of the following form:

$$F=-k_0(M^*+M)(1+\bar{k}_C\kappa)\,,\qquad \text{where:}\quad \kappa=\nabla\cdot\frac{\nabla\phi}{|\nabla\phi|}\,. \tag{5}$$

The reaction rate equation (5) models three gel-tissue interaction mechanisms that are based on the following assumptions:

— At $t=0$ the cartilage cells "detect" the presence of the (foreign) hydrogel. In response to this phenomenon, the initial interface reaction rate is k_0M^*, where M^* is the homeostatic matrix density of native cartilage in the tissue explant.

— For $t>0$, the interface reaction rate increases in proportion to the concentration of net accumulated ECM $M(r,z,t)$ in the vicinity of the interface.

— The interface reaction rate also increases with the mean curvature κ along the interface since the local hydrogel volume will be exposed to a greater cell density (per unit volume) as κ increases (Figure 2). An additional curvature parameter $\bar{k}_C$ is introduced to model this phenomenon.

The governing equations for our level set reaction-diffusion model consist of equations (1)-(5). To model the in-vitro cartilage regeneration experiment, the initial conditions are taken as $(0<z<h)$:

$$N(r,z,0)=\begin{cases} N_H & 0<r<a\,,\\ N^* & a<r<b\,,\end{cases}\qquad M(r,z,0)=0,\ \ 0<r<b\,, \tag{6}$$

where N_H is the initial nutrient concentration of the (nutrient-rich) hydrogel, and it is typically the case that $N_H >> N^*$. The second condition in (6) corresponds to the assumption that, prior to defect filling, the cartilage explant is in homeostasis and, thus, there is no net ECM synthesis in this initial state. Initially, the gel-tissue interface is assumed to be located along the surface $r=a$ and corresponds to the level set $\phi(a,z,0)=0$ (Figure 1). Over the entire

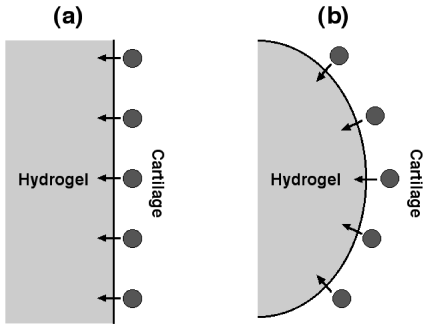

Figure 2: Illustration of the effect of local mean curvature of the gel-tissue interface on the local reaction. (a) Zero curvature case ($\kappa = 0$) (b) For $\kappa > 0$ the local hydrogel is exposed to increased cellular biosynthesis (per unit volume).

domain, the level set function is initialized as ($0 < z < h$):

$$\phi(r, z, 0) = \begin{cases} -d(r, z) & \text{for } 0 \leq r < a\,, \\ 0 & \text{for } r = a\,, \\ d(r, z) & \text{for } a < r \leq b\,, \end{cases} \tag{7}$$

where $d(r, z)$ is the minimum distance to the interface.

We assume that the two exposed surfaces of the gel-tissue aggregate ($r = b$ and $z = h$) are maintained at a fixed concentration. Two cases are considered, corresponding to immersion of the aggregate in either a solution at homeostatic concentration N^*, or at a nutrient-rich concentration equivalent to N_H (e.g. [27]). In the experiment, these conditions can be achieved via periodic exchange of media surrounding the sample on a time scale that is much shorter than the overall tissue regeneration time. These two surfaces are also assumed to be impermeable to flux of newly synthesized ECM, giving rise to zero normal flux (Neumann) boundary conditions for M. Along the two remaining boundaries, $r = 0$ and $z = 0$, zero normal flux conditions are prescribed for both dependent variables due to the assumptions of axial symmetry and an impermeable platen, respectively. It is noted that the impermeable platen supporting the sample is also a first approximation of an in-vivo setting in which the osteochondronal defect penetrates to the bone, which has low permeability relative to the hydrogel.

2.3. Nondimensionalization

To facilitate analysis of interaction between the mechanisms in the model, the following dimensionless variables are introduced

$$\bar{t} = \frac{tD_N^{(1)}}{b^2}, \quad \bar{r} = \frac{r}{b}, \quad \bar{z} = \frac{z}{b}, \quad \bar{N} = \frac{N}{N^*}, \quad \bar{M} = \frac{M}{M^*}, \quad \bar{\phi} = \frac{\phi}{b}. \tag{8}$$

Transformation of (1)-(5) using (8), yields the following nondimensional governing equations ($0 < \bar{r} < 1,\ 0 < \bar{z} < h/b,\ \bar{t} > 0$):

$$\frac{\partial \bar{N}}{\partial \bar{t}} = \bar{\delta}_N^{(i)} \left(\frac{\partial^2 \bar{N}}{\partial \bar{r}^2} + \frac{1}{\bar{r}} \frac{\partial \bar{N}}{\partial \bar{r}} + \frac{\partial^2 \bar{N}}{\partial \bar{z}^2} \right) - \bar{\gamma}_N^{(i)} \left(\bar{N} - 1 \right), \tag{9}$$

$$\frac{\partial \bar{M}}{\partial \bar{t}} = \bar{\delta}_M^{(i)} \left(\frac{\partial^2 \bar{M}}{\partial \bar{r}^2} + \frac{1}{\bar{r}} \frac{\partial \bar{M}}{\partial \bar{r}} + \frac{\partial^2 \bar{M}}{\partial \bar{z}^2} \right) + \bar{\gamma}_M^{(i)} \left(\bar{N} - 1 \right), \tag{10}$$

$$\frac{\partial \bar{\phi}}{\partial \bar{t}} - \bar{\eta}(1 + \bar{M})(1 + \bar{k}_C \kappa) |\nabla \bar{\phi}| = 0. \tag{11}$$

Equations (9)-(11) involve the set of nondimensional parameters consisting of $h/b,\ a/b,\ \bar{k}_C, N_H/N^*$ and:

$$\bar{\gamma}_N^{(i)} = \frac{k_N^{(i)} b^2}{D_N^{(1)}}, \quad \bar{\gamma}_M^{(i)} = \frac{k_M^{(i)} b^2}{D_N^{(1)}}, \quad \bar{\eta} = \frac{k_o M^* b}{D_N^{(1)}}, \quad \bar{\delta}_N^{(i)} = \frac{D_N^{(i)}}{D_N^{(1)}}, \quad \bar{\delta}_M^{(i)} = \frac{D_M^{(i)}}{D_N^{(1)}}. \tag{12}$$

The assumptions $k_N^{(1)} = 0 = k_M^{(1)}$ in (2)-(3) imply that $\bar{\gamma}_N^{(1)} = 0 = \bar{\gamma}_M^{(1)}$ in (12), resulting in a total of 10 nondimensional parameters in the model (note that $\bar{\delta}_N^{(1)} = 1$). Transformation of the initial conditions (6)-(7) yields ($0 < \bar{z} < h/b$):

$$\bar{N}(\bar{r}, \bar{z}, 0) = \begin{cases} N_H/N^* & 0 < \bar{r} < a/b, \\ 1 & a/b < \bar{r} < 1, \end{cases} \qquad \bar{M}(\bar{r}, \bar{z}, 0) = 0, \ \ 0 < \bar{r} < 1, \tag{13}$$

$$\bar{\phi}(\bar{r}, \bar{z}, 0) = \begin{cases} -d(\bar{r}, \bar{z}) & \text{for } 0 < \bar{r} < a/b, \\ 0 & \text{for } \bar{r} = a/b, \\ d(\bar{r}, \bar{z}) & \text{for } a/b < \bar{r} < 1. \end{cases} \tag{14}$$

Transformation of the boundary conditions results in prescribing a fixed value of the nutrient concentration (either 1 or N_H/N^*) on the surfaces $\bar{r} = 1$ and $\bar{z} = h/b$, while all other, zero-flux, boundary conditions are mathematically equivalent in the transformed variables.

3. Numerical Methods

3.1. Mesh and Level Set Considerations

The gel-tissue aggregate was modeled as a cylindrical domain with $h/b = 1$ and $a/b = 0.5$. This domain was discretized using a uniform mesh consisting of 256×256 grid points. The diffusion coefficient is determined by noting the sign of the level set function and using the appropriate diffusion coefficient. For grid points near the interface, the diffusion coefficients are determined via interpolation [13] and, specifically, a hyperbolic tangent function was used.

3.2. Finite Difference Scheme

The reaction-diffusion equations (9)-(10) were discretized using a (fully implicit) backward Euler scheme that is first-order accurate in time and second-order accurate in space. Denote $(\cdot)_{ij}^n = (\cdot)(i\Delta\bar{r}, j\Delta\bar{z}, n\Delta\bar{t})$. To discretize (11), we used the first-order entropy-satisfying upwind viscosity schemes presented by Sethian [30], which approximate derivatives by biasing the finite difference stencil in the direction of characteristic information. For axisymmetric geometry, the level set equation (11) was discretized in the following manner [30]:

$$\bar{\phi}_{ij}^{n+1} = \bar{\phi}_{ij}^n + \Delta\bar{t}\,[\max(\bar{F}_{ij}^n, 0)\nabla^+\bar{\phi} + \min(\bar{F}_{ij}^n, 0)\nabla^-\bar{\phi}] \tag{15}$$

From (11), $\bar{F}_{ij}^n$ in (15) is given by:

$$\bar{F}_{ij}^n = \bar{\eta}(1 + \bar{M}_{ij}^n)(1 + \bar{k}_C\kappa_{ij}^n) \tag{16}$$

and, for axisymmetric geometry, κ in (5) is:

$$\kappa = \frac{\bar{\phi}_{\bar{z}\bar{z}}\bar{\phi}_{\bar{r}}^2 - 2\bar{\phi}_{\bar{r}}\bar{\phi}_{\bar{z}}\bar{\phi}_{\bar{r}\bar{z}} + \bar{\phi}_{\bar{r}\bar{r}}\bar{\phi}_{\bar{z}}{}^2}{\left(\bar{\phi}_{\bar{r}}^2 + \bar{\phi}_{\bar{z}}^2\right)^{3/2}}, \tag{17}$$

where, for brevity, the subscripts denote partial differentiation. Curvature on the mesh was calculated explicitly in time, i.e. as κ_{ij}^n, via (17) using centered difference rules for all spatial derivatives. The gradients in (15) are defined as [30]:

$$\nabla^+\bar{\phi} = [\max(D_{ij}^{-\bar{r}}, 0)^2 + \min(D_{ij}^{+\bar{r}}, 0)^2 + \max(D_{ij}^{-\bar{z}}, 0)^2 + \min(D_{ij}^{+\bar{z}}, 0)^2]^{1/2}, \tag{18}$$

$$\nabla^-\bar{\phi} = [\max(D_{ij}^{+\bar{r}}, 0)^2 + \min(D_{ij}^{-\bar{r}}, 0)^2 + \max(D_{ij}^{+\bar{z}}, 0)^2 + \min(D_{ij}^{-\bar{z}}, 0)^2]^{1/2}, \tag{19}$$

where $D_{ij}^{\pm\bar{r}}$ and $D_{ij}^{\pm\bar{z}}$ are the standard first-order finite difference rules for first derivatives in the $\bar{r}$ and $\bar{z}$ directions, respectively. In enforcing (15) at boundary nodes, the mesh was extended by one additional node to provide a value for the

level set function in the spatial difference rules, and was set equal to the value at the adjacent node.

This discretization has a time step restriction based on the mathematical form of $\bar{F}_{ij}^n$ in (16). When curvature effects are not considered ($\bar{k}_C = 0$), the condition is [29]:

$$\Delta\bar{t}\left(\frac{\max\{\bar{F}\}}{(\Delta\bar{r})}+\frac{\max\{\bar{F}\}}{(\Delta\bar{z})}\right)<1\,. \tag{20}$$

When curvature effects are included ($\bar{k}_C \neq 0$), equation (15) has a parabolic component and the time step restriction is:

$$\Delta\bar{t}\left(\frac{\max\{\bar{F}\}}{(\Delta\bar{r})^2}+\frac{\max\{\bar{F}\}}{(\Delta\bar{z})^2}\right)<1\,, \tag{21}$$

where $\bar{F}$ is determined via (16) over the duration of the simulation. In practice, satisfaction of (20)-(21) was enforced by refining spatial and temporal step sizes until it was ensured that conditions (20)-(21) were not violated at any point during the numerical solution.

To improve computational efficiency, a narrow-band level set method was implemented to avoid evaluation of the level set function $\bar{\phi}$ on the entire domain at each time step. Briefly, in this technique a narrow band is created around the interface $\bar{\phi} = 0$, and only grid points within this band are evaluated and updated at each time step. Grid points outside the narrow band are given a fixed value based on neighboring values of the signed distance function within the narrow band. As the interface propagates through the domain, the narrow band region is continually updated.

4. Results

4.1. Parametric Analysis

For all numerical simulations, the geometry of the aggregate was set at $a/b = 0.5$ and $h/b = 1$. In (12), $\bar{\delta}_N^{(1)} \equiv 1$ (by definition) and the three non-dimensional parameters $\bar{\delta}_N^{(2)}, \bar{\delta}_M^{(1)}, \bar{\delta}_M^{(2)}$ are determined by relative diffusivities of nutrients and matrix constituents in the cartilage and hydrogel regions. These values were estimated based on diffusion coefficients for dextrans of varying molecular weight that have been measured using fluorescence microscopy with photobleaching [8, 18]. Specifically, in [18], the diffusion coefficients of dextrans in photocrosslinkable hyaluron hydrogels were found to lie in the range of 600-

$8000\mu m^2/s$, with diffusivities decreasing as solute molecular weight was increased in a range of 3 to 500kDa. Based on these findings, a reference value of $D_N^{(1)} = 8000\mu m^2/s$ was chosen for the nutrient diffusion coefficient in the hydrogel region. The matrix diffusion coefficient in the hydrogel region was assumed to be one order of magnitude smaller, i.e. $D_M^{(1)} = D_N^{(1)}/10$. In the cartilage region, coefficients were estimated based on [8], in which similar photobleaching techniques were used to measure diffusion coefficients of fluorescent dextrans (3-500kDa) in porcine articular cartilage. The range of diffusion coefficients in mid-zone cartilage was roughly 5-70$\mu m^2/s$, again, exhibiting a decreasing trend as solute molecular weight increased. Based on these collective findings, the nondimensional diffusion coefficients in our model were approximated to have the following fixed values:

$$\bar{\delta}_N^{(1)} \equiv 1, \quad \bar{\delta}_N^{(2)} = \frac{D_N^{(2)}}{D_N^{(1)}} = 0.01, \quad \bar{\delta}_M^{(1)} = \frac{D_M^{(1)}}{D_N^{(1)}} = 0.1, \quad \bar{\delta}_M^{(2)} = \frac{D_M^{(2)}}{D_N^{(1)}} = 0.001. \quad (22)$$

Since hydrogels are nutrient rich, the initial hydrogel nutrient concentration (N_H) was taken to be one order of magnitude larger than the cartilage nutrient concentration at homestasis (N^*), so that $N_H/N^* = 10$. The remaining parameters in the model are $\bar{\gamma}_N^{(2)}$, $\bar{\gamma}_M^{(2)}$, $\bar{\eta}$ and $\bar{k}_C$, which govern, respectively, the cell biological mechanisms of nutrient absorption, matrix biosynthesis, interfacial hydrogel degradation and effects of curvature on the interfacial reaction rate.

Results presented in the following sections illustrate effects of these four parameters on tissue regeneration times in the gel-tissue aggregrate. While the primary focus is on the zero-curvature case ($\bar{k}_C = 0$), some effects of curvature are also illustrated in Section 4.3. At present, detailed data for the cartilage regeneration experiment is not available. Limited studies in which cells are seeded directly in hydrogels indicate that regeneration times for complete gel degradation may be on the order of weeks to months [2]. Consequently, 8 representative cases were chosen for simulation (Table 1), based on illustrating various degrees of coupling among mechanisms in the model, and rough calibration of tissue regeneration times in the appropriate range. In each of the 8 cases, in-vitro experiments were simulated for two types of boundary conditions. In the first case (called BC1), boundary conditions for non-dimensional nutrient concentration $\bar{N}$ were set to 1 at upper surface ($\bar{z} = h/b$) and the peripheral surface ($\bar{r} = 1$), corresponding to the case of immersion in media maintained at conditions associated with cartilage homeostasis. In the second case (called BC2), boundary conditions for non-dimensional nutrient concentrations along these surfaces were set at N_H/N^*, to model the case of nutrient-rich media.

Case	BC	$\bar{\eta}$	$\bar{\gamma}_M^{(2)}$	$\bar{\gamma}_N^{(2)}$	Case	BC	$\bar{\eta}$	$\bar{\gamma}_M^{(2)}$	$\bar{\gamma}_N^{(2)}$
I	1	0.001	0.01	0.01	V	2	0.001	0.01	0.01
II	1	0.001	1	0.01	VI	2	0.001	1	0.01
III	1	0.005	0.01	0.01	VII	2	0.005	0.01	0.01
IV	1	0.005	1	0.01	VIII	2	0.005	1	0.01

Table 1: Representative cases for parametric analysis of the cartilage regeneration model

4.2. Simulations

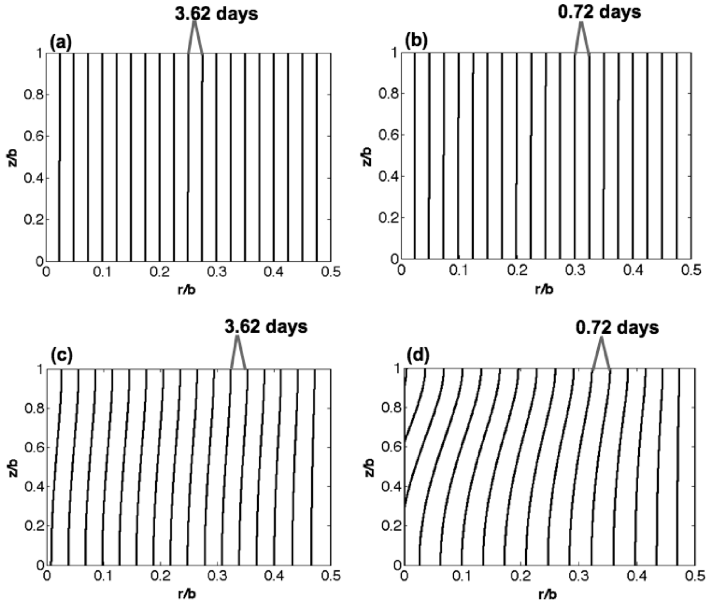

Figure 3: Simulations of the evolving gel-tissue interface $\bar{\phi}(\bar{r}, \bar{z}, \bar{t}) = 0$ when the aggregate is immersed in media maintained at homeostatic nutrient concentration N^* (BC1). (a) Case I, (b) Case III, (c) Case II, (d) Case IV (see Table 1 for parameter values).

Motion of the gel-tissue interface was simulated in the case of immersion in media at homeostatic nutrient concentration, as shown in Figure 3 for cases I-IV. In cases I and III, where the nutrient absorption rate ($\bar{\gamma}_N^{(2)} = 0.01$) and

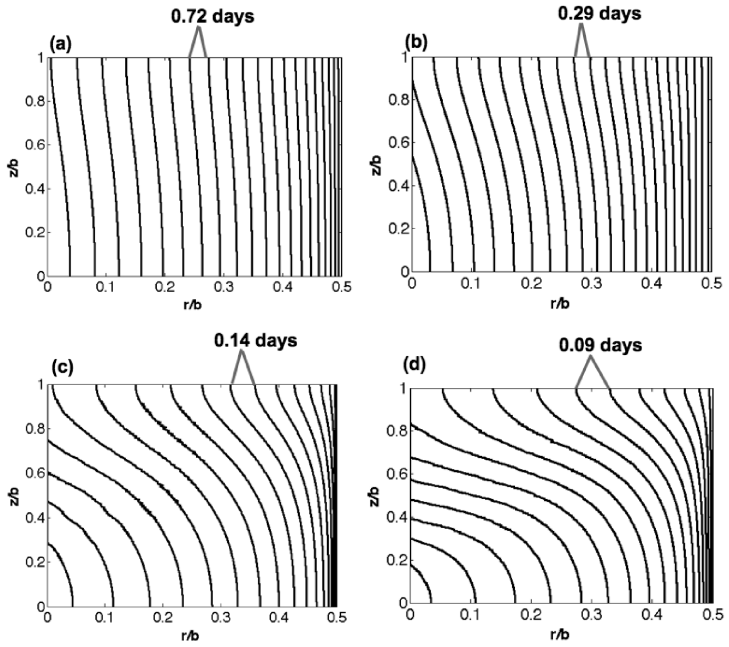

Figure 4: Simulations of the evolving gel-tissue interface, $\bar{\phi}(\bar{r}, \bar{z}, \bar{t}) = 0$ when the aggregrate is immersed in nutrient-rich media maintained at the initial hydrogel concentration N_H (BC2). (a) Case V, (b) Case VII, (c) Case VI, (d) Case VIII (see Table 1 for parameter values).

matrix synthesis rate ($\bar{\gamma}_M^{(2)} = 0.01$) are small, the interface maintains a roughly vertical shape, with the rate of propagation being proportional to the interface parameter $\bar{\eta}$ (Figure 3a,b). As the matrix synthesis rate is increased to $\bar{\gamma}_M^{(2)} = 1$, spatial gradients in nutrient concentration affect the shape and propagation of the gel-tissue interface (Figure 3c,d). Points along the interface that are closer to the lower, impermeable, tissue boundary ($z = 0$) advance at a faster rate than points near the top surface ($z = h$), where a concentration of N^* is maintained, due to the fact that $N_H >> N^*$.

Similarly, motion of the gel-tissue interface was simulated under a second set of boundary conditions (BC2), corresponding to immersion of the aggregate in nutrient-rich media maintained at the initial hydrogel nutrient concentration N_H (Figure 4). For these cases V-VIII, spatial gradients in nutrient concentration have a greater influence on the shape of the interface at earlier times due to the high contrast between the initial nutrient concentration in the cartilage

region (N^*) and the external nutrient concentration in the bath (N_H). In contrast to BC1 (Figure 3), the availability of more nutrients near the permeable surface of the aggregate ($z = h$) results in faster advancement of points that are closer to the top. As the matrix synthesis rate is increased from $\bar{\gamma}_M^{(2)} = 0.01$ (V and VII) to $\bar{\gamma}_M^{(2)} = 1$ (VI and VIII), simulations exhibit a high degree of coupling among the underlying reactive and diffusive mechanisms that result in more complex shapes of the gel-tissue interface as cartilage is regenerated in the hydrogel region (Figure 4c,d).

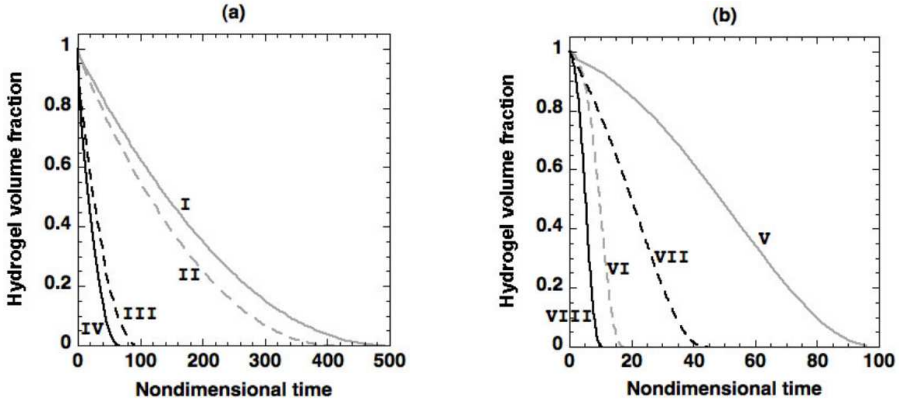

Figure 5: Simulations of hydrogel degradation, relative to initial hydrogel volume, in a gel-tissue aggregate immersed in media maintained at: (a) the homeostatic nutrient concentration N^* (BC1), (b) the nutrient-rich concentration N_H (BC2) (see Table 1 for parameter values).

The *regeneration time*, or the amount of time required for the cartilage to degrade and turnover the entire hydrogel region, is a primary variable of interest to the experimentalist. To illustrate dependence on parameters in our model, depletion of hydrogel volume, relative to its initial value in the gel-tissue aggregate, was determined as a function of nondimensional time (Figure 5) for the 8 cases of Table 1. When the aggregate is immersed in media maintained at the homeostatic nutrient concentration N^* (Figure 5a), it is observed that the regeneration time is more sensitive to changes in the interface reaction rate $\bar{\eta}$ as compared to changes in the matrix synthesis rate $\bar{\gamma}_M^{(2)}$, i.e. I/II versus III/IV. In particular, for a fixed value of $\bar{\eta}$, increasing the value of the matrix synthesis rate $\bar{\gamma}_M^{(2)}$ by a factor of 100, increases the regeneration rate (e.g. I/II in Figure 5a), but this dependence is much less sensitive than for an increase in the interface parameter $\bar{\eta}$ by a factor of 5. In contrast, when the aggregate is immersed in

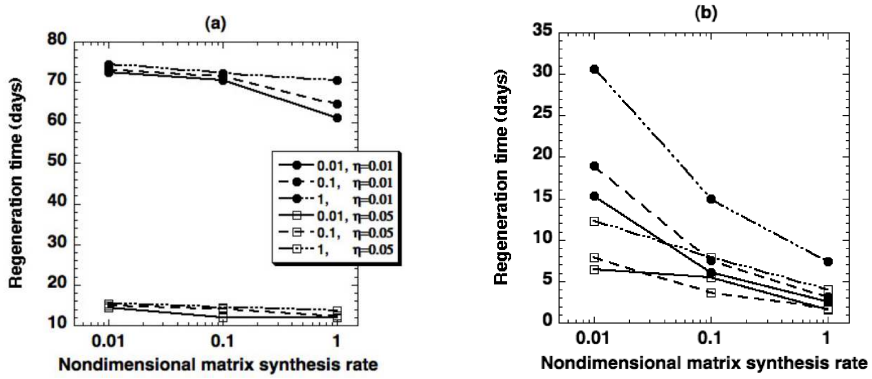

Figure 6: Parametric analysis of cartilage regeneration times (in days) for a gel-tissue aggregate immersed in media maintained at: (a) the homeostatic nutrient concentration N^* (BC1), (b) the nutrient-rich concentration N_H (BC2). Parametric dependence on $\bar{\gamma}_M^{(2)}$ is shown on the x-axis, while dependence on $\bar{\gamma}_N^{(2)}$ and $\bar{\eta}$ is shown in the legend

nutrient-rich media (Figure 5b), regeneration times are significantly smaller due to the availability of nutrients in the external solution that stimulate cellular biosynthesis of matrix constituents. Regeneration curves exhibit a different shape, and greater sensitivity is exhibited with respect to both parameters, with regeneration times significantly reduced when either $\bar{\gamma}_M^{(2)}$ or $\bar{\eta}$ are increased.

The model was also used to determine the parametric dependence of cartilage regeneration times, in days, on the biological reaction parameters $\bar{\gamma}_N^{(2)}$, $\bar{\gamma}_M^{(2)}$ and $\bar{\eta}$, and 36 unique cases were simulated (Figure 6). Nondimensional regeneration times were computed as the time required for the hydrogel volume to decrease to 1% of its initial value. Based on (8), and the fixed parameter values (Section 4.1), the conversion factor from nondimensional time units to physical units (in days) was 0.145. Use of the model in such parametric analyses provides insight on the relative contribution and coupling of the underlying biophysical and cell biological mechanisms to the overall cartilage regeneration time.

4.3. Effects of Curvature

Along the gel-tissue interface, the local shape of the interface can influence the rate of the reaction by which hydrogel is depleted and replaced with newly

synthesized cartilage. This effect was modeled via the term involving the local mean curvature κ in (11). Initially, $\kappa = 0$ along the entire gel-tissue interface (Figure 2a). As time evolves, concentration gradients give rise to local changes in the shape of the interface. These local changes, effectively, increase ($\kappa > 0$, Figure 2b) or decrease ($\kappa < 0$) the rate of reaction between the hydrogel and nearby cartilage cells that results in gel degradation and replacement with new tissue. To illustrate effects of curvature, the case $\bar{k}_C = 0.1$ was considered.

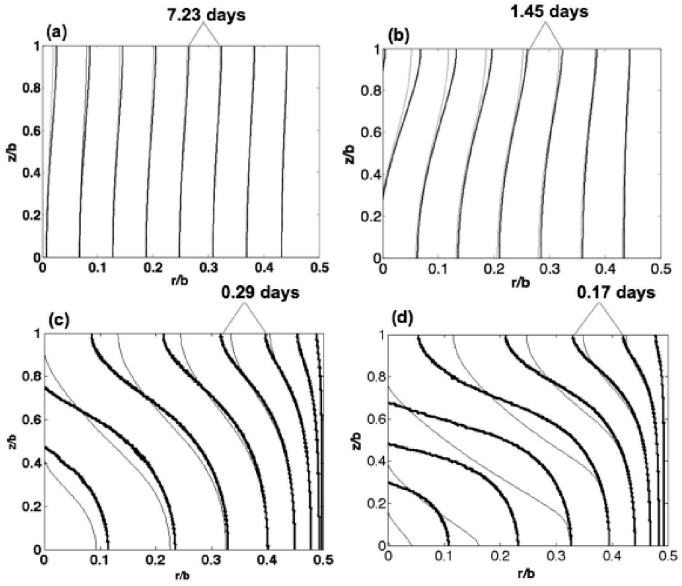

Figure 7: Representative simulations of the evolving gel-tissue interface $\bar{\phi}(\bar{r}, \bar{z}, \bar{t}) = 0$ in the cases $\bar{k}_C = 0$ (black) and $\bar{k}_C = 0.1$ (gray). Results are illustrated when the aggregate is immersed in media maintained at (i) homeostatic nutrient concentration N^*: (a) Case II, (b) Case IV, and (ii) the nutrient-rich initial hydrogel concentration N_H: (c) Case VI, (d) Case VIII (see Table 1)

An illustration of the effect of including curvature in the model is shown in Figure 7 for 4 representative cases of Table 1 where the matrix synthesis rate is $\bar{\gamma}_M^{(2)} = 1$. In cases II and IV (Figure 7a,b), where the aggregate is immersed in media at homeostatic nutrient concentration N^*, curvature effects are minimal relative to the other mechanisms in our model. By contrast, in cases VI and VIII (Figure 7c,d), where the aggregate is immersed in nutrient-rich media, curvature effects are significant. For example, in case VIII (Figure 7d) regions of positive

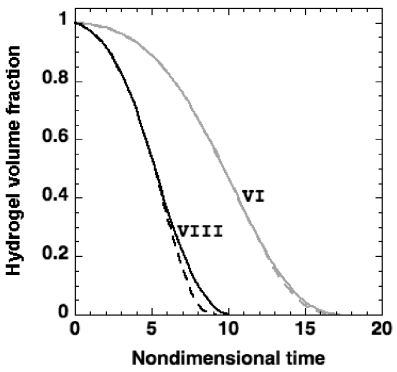

Figure 8: Simulations of hydrogel degradation for cases VI (gray) and VIII (black) of Table 1 in the cases $\bar{k}_C = 0$ (dashed) and $\bar{k}_C = 0.1$ (solid).

curvature ($\kappa > 0$) cause the gel-tissue interface to propagate faster than for the zero-curvature model. Similarly, the opposite effects is observed in regions of negative curvature. However, even for cases VI and VIII, the overall effects of curvature on tissue regeneration times are small due to counterbalancing of effects of regions of positive and negative curvature in the instantaneous profiles of the evolving gel-tissue interface (Figure 8). Nevertheless, incorporation of curvature effects into the cartilage regeneration model may be appropriate for experiments where the tissue exhibits structural inhomogeneities that are observed to effect the spatial nature of the tissue regeneration. An example of such an inhomogeneity in articular cartilage is the depth dependent variation in ECM fiber orientation, where the mid-zone is generally isotropic, while the surface and deep zones have preferential tangential and normal orientations, respectively.

5. Summary

The mathematical model presented in this study provides a simplified framework for modeling several key biophysical mechanisms involved in interactions between cartilagenous tissues and natural or synthetic polymer scaffold materials. Experimental analysis of the cartilage regeneration problem can be time intensive and challenging, given the multitude of possible polymeric hydrogel designs, the lengthy time scale required to achieve complete regeneration, and

limitations of current experimental techniques. In this context, models of various biophysical and biomechanical aspects of tissue regeneration can serve as beneficial tools for experimental design that can, potentially, reduce the time required to achieve optimal functional outcomes. Among the many possible extensions of the current model, some examples include delineation of variables for the nutrient species (e.g. glucose, oxygen) and the synthesized ECM constituents (e.g. collagen, glycosaminoglycan), and incorporation of additional effects such as seeding the hydrogel with cells, saturation in cellular absorption of nutrients, and mechanical factors involved in assembly of newly synthesized ECM into a cross-linked network. Further experimental studies and development of novel experimental techniques will greatly facilitate the realization of an accurate, extended model of the cartilage regeneration problem incorporating these effects.

Acknowledgments

The authors would like to thank L.A. Setton for helpful discussions, and acknowledge research support from NSF (DMS-0636590) and NIH (AG15768).

References

[1] C. Archer, P. West, Cells in focus: the chondrocyte, *Int. J. Biochem.*, **35** (2003), 401-404.

[2] S. Bryant, K. Anseth, Controlling the spatial distribution of ECM components in degradable PEG hydrogels for tissue engineering cartilage, *J. Biomed. Mater. Res. Part A*, **64A** (2003), 70-79.

[3] H. Betre, L. Setton, D. Meyer, A. Chilkoti, Characterization of a genetically engineered elastin-like polypeptide for cartilaginous tissue repair, *Biomacromolecules*, **3** (2002), 910-916.

[4] J. Buckwalter, Articular cartilage, *Instructional Course Lectures*, **32** (1983), 349-370.

[5] F. Coletti, S. Macchietto, N. Elvassore, Mathematical modeling of three-dimensional cell cultures in perfusion bioreactors, *Ind. Eng. Chem. Res.*, **45** (2006), 8158-8169.

[6] J. Dunn, W. Chan, V. Cristini, J. Kim, J. Lowengrub, S. Singh, B. Wu, Analysis of cell growth in three-dimensional scaffolds, *Tissue Eng.*, **12** (2006), 705-716.

[7] J. Elisseeff, K. Anseth, D. Sims, W. Mcintosh, M. Randolph, M Yaremchuk, R. Langer, Transdermal photopolymerization of poly(ethylene oxide)-based injectable hydrogels for tissue-engineered cartilage, *Plast. Reconst. Surg.*, **104** (1999), 1014-1022.

[8] H. Leddy, F. Guilak, Site-specific molecular diffusion in articular cartilage measured using fluorescence recovery after photobleaching, *Ann. Biomed. Eng.*, **31** (2003), 753-760.

[9] K. Davis, J. Burdick, K. Anseth, Photoinitiated crosslinked degradable copolymer networks for tissue engineering applications, *Biomat.*, **24** (2003), 2485-2495.

[10] M. Dimicco, R. Sah, Dependence of cartilage matrix composition on biosynthesis, diffusion, and reaction, *Transp. Porous Media*, **50** (2002), 57-73.

[11] C. Galban, B. Locke, Analysis of cell growth in a polymer scaffold using a moving boundary approach, *Biotech. Bioeng.*, **56** (1997), 422-432.

[12] T. Karande, J. Ont, C. Agrawal, Diffusion in musculoskeletal tissue engineering scaffolds: design issues related to porosity, permeability, architecture, and nutrient mixing, *Ann. Biomed. Eng.*, **32** (2004), 1728-1743.

[13] Y. Kim, N. Goldenfeld, Computation of dendritic microstructures using a level set method, *Phys. Rev. E*, **62** (2000), 2471-2474.

[14] C. Kirkpatrick, V. Krump-Konvalinkova, R. Unger, F. Bittinger, M. Otto, K. Peters, Tissue response and biomaterial integration: the efficacy of in vitro methods, *Biomol. Eng.*, **19** (2002), 211-217.

[15] G. Lemon, J. King, H. Byrne, O. Jensen, K. Shakesheff, Mathematical modeling of engineered tissue growth using a multiphase porous flow mixture theory, *J. Math. Bio.*, **52** (2006), 571-594.

[16] A. Mak, The apparent viscoelastic behavior of articular cartilage – the contributions from the intrinsic matrix viscoelasticity and interstitial fluid flows, *J. Biomech. Eng.*, **108** (1986), 123-130.

[17] V. Mow, A. Ratcliffe, Structure and function of articular cartilage and meniscus, In: *Basic Orthopaedic Biomechanics* (Ed-s: V.C. Mow, W. Hayes), Raven Press, New York (1991), 113-177.

[18] D. Nettles, T. Parker Vail, M. Morgan, M. Grinstaff, L. Setton, Photocrosslinkable hyaluronan as a scaffold for articular cartilage repair, *Ann. Biomed. Eng.*, **32** (2004), 391-397.

[19] K. Nguyen, J. West, Photopolymerizable hydrogels for tissue engineering applications, *Biomaterials*, **23** (2002), 4307-4314.

[20] B. Obradovic, J. Meldon, L. Freed, Glycosaminoglycan deposition in engineered cartilage: experiments and mathematical model, *Am. Inst. of Chem. J.*, **46** (2000), 1860-1871.

[21] S. Osher, R. Fedkiw, *Level Set Methods and Dynamic Implicit Surfaces*, Springer-Verlag, New York, (2003).

[22] C. Ossendorf, C. Kaps, P. Kreuz, G. Burmester, M. Sittinger, C. Erggelet, Treatment of posttraumatic and focal osteoarthritic cartilage defects of the knee with autologous polymer-based three-dimensional chondrocyte grafts: 2-year clinical results, *Arthritis Res. Ther.*, **9** (2007).

[23] Y. Park, M. Lutolf, J. Hubbel, E. Hunziker, M. Wong, Bovine primary chondrocyte culture in synthetic matrix metalloproteinase sensitive poly(ethylene glycol)-based hydrogels as a scaffold for cartilage repair, *Tissue Eng.*, **10** (2004), 512-522.

[24] A. Rydholm, C. Bowman, K. Anseth, Degradable thilo-acrylate photopolymers: polymerization and degradation behavior of an in situ forming biomaterial, *Biomaterials*, 26(2005), 4495-4906.

[25] Sarzi-Puttini, M. A. Cimmino, R. Scarpa, R. Caporali, F. Parazzini, A. Zaninelli, F. Atzen, C. Bianca, Osteoarthritis: an overview of the disease and its treatment strategies, *Semin. Arthritis Rheum*, **35** (2005), 1-10

[26] B. Sengers, C. Donkelaar, C. Oomens, F. Baaijens, Computational study of culture conditions and nutrient supply in cartilage tissue engineering, *Biotechnol. Progr.*, **21** (2005), 1252-1261.

[27] B. Sengers, H. Heywood, D. Lee, C. Oomens, D. Bader, Nutrient utilization by bovine articular chondrocytes: a combined experimental and theoretical approach, *Trans. Am. Soc. Mech. Eng.*, **127** (2005), 758-766.

[28] B. Sengers, C. Van Donkelaar, C. Oomens, F. Baaijens, The local matrix distribution and the functional development of tissue engineered cartilage, a finite element study, *Annals of Biomed. Eng.*, **32** (2004), 1718-1727.

[29] J. Sethian, *Level Set Methods: Evolving Interfaces in Geometry, Fluid Dynamics and Materials Science*, Cambridge University Press, Cambridge (1996).

[30] J. Sethian, Evolution, Implementation and application of level set and fast marching methods for advancing fronts, *J. of Comput. Phys.*, **169** (2005), 503-555.

[31] R. Tuli, W. Li, R. Tuan, Current state of cartilage tissue engineering, *Arthritis Res. Ther.*, **5** (2003), 235-238.

[32] J. Urban, Present perspectives on cartilage and chondrocyte mechanobiology, *Biorheology*, **37** (2000), 185-190.

[33] C. Wilson, L. Bonassar, S. Kohles, Modeling the dynamic composition of engineered cartilage, *Arch. Biochem. Biophys.*, **408** (2002), 246-254.

[34] D. Wilson, J. King, H. Byrne, Modelling scaffold occupation by a growing, nutrient-rich tissue, *Math. Model Meth. Appl. Sci.*, **17** (2007), 1721-1750.

[35] K. Yang. D. Saris, W. Dhert, A. Verbout, Osteoarthritis of the knee: current treatment options and future directions, *Curr. Orthopaed.*, **18** (2004), 311-320.